Draft version May 15, 2021
Typeset using LaTeX **twocolumn** style in AASTeX631

Morphologies of Ultra-Faint Dwarf Galaxies as a Window into the Dark Matter Universe and Galaxy Formation

by

Molly Childers
Instructor: Nitya Kallivayalil

This thesis is submitted in partial completion of the requirements of the BA Astronomy Major.

Department of Astronomy
University of Virginia
May 15, 2021

Draft version May 15, 2021
Typeset using LaTeX **twocolumn** style in AASTeX631

Morphologies of Ultra-Faint Dwarf Galaxies as a Window into the Dark Matter Universe and Galaxy Formation*

Molly J. S. Childers,[1] Nitya Kallivayalil,[1] and Hannah Richstein[1]

[1] *Department of Astronomy, University of Virginia, 530 McCormick Road, Charlottesville, VA 22904, USA*

ABSTRACT

We explore the morphologies of ultra-faint dwarf galaxies in order to get a window into how to use their structures to place constraints on major components of universe. Characteristics of ultra-faint dwarf galaxies in our own galactic neighborhood give us valuable insight into the history of galaxy formation and the role dark matter plays in the evolution of our universe. We first used Hubble Space Telescope images to determine masking coordinates that will help further analyze galaxy data, and then we recreated color-magnitude diagrams and isochrones from the Hercules galaxy to confirm their accuracy. Finally, we tested the effect of modifying initial structural parameters in a Markov Chain Monte Carlo program for two galaxies, Eridanus II and Pegasus III, and found that changing position angle and normalization profile had the largest effect on half-light radius while decreasing magnitude depth led to larger position angles, ellipticities, and half-light radii independent of profile type. Next steps would be to analyze these results in detail and determine which profile type fits a given galaxy better.

Keywords: ultra-faint dwarf galaxies - dark matter - position angle - ellipticity - half-light radius / extension

1. INTRODUCTION

Satellite dwarf galaxies in the Milky Way halo give a glimpse into the structure of our universe by providing valuable information about dark matter physics. Dark matter halos accumulate their mass due to the accretion of smaller objects (Kallivayalil et al. 2018). A sample of ultra-faint, low mass galaxies around the Milky Way (Bechtol et al. 2015; Drlica-Wagner et al. 2015; Koposov et al. 2015a; Martin et al. 2015; Laevens et al. 2015a; Torrealba et al. 2016a,b, 2018; Koposov et al. 2015a; Kim et al. 2015; Drlica-Wagner et al. 2016; Koposov et al. 2018; Homma et al. 2018) give us insight into this accretion of our own halo, and as a result, tells us more about the mysteries of dark matter. This catalog of dwarf galaxies has a range of half-light radii $r_h = 0.4 - 31.2$ arcminutes and magnitudes from $M_V = 2 - 8$ (Kallivayalil et al. 2018). The two galaxies examined more closely in this paper, Eridanus II and Pegasus III, have sizes $r_h = 1.5$ and $r_h = 0.8$ and magnitudes $M_V = -6.6$ and $M_V = -3.4$, respectively.

* Released on May, 15, 2021

2. DATA

When working with this sample of ultra-faint dwarf galaxies, we first analyzed images obtained by the Hubble Space Telescope (HST) and determined which regions of these images had galaxy data and which did not by masking out certain fields. We then took a closer look at the Hercules, Eridanus II, and Pegasus III galaxies and created plots to visualize important characteristics that tell us more about their makeups and histories.

2.1. *Masking*

The first task was to take HST images of the ultra-faint dwarf galaxies and use the SAOImageDS9 application to obtain coordinates to be used for data masking. Due to chip gaps, saturated stars, and diffraction spikes, parts of these data sets need to be masked so as not to affect their morphologies. The coordinates obtained were the four corners of each image, the four corners of the chip gap from the telescope, the center and radius of any saturated stars, and the north-south and east-west coordinates of any large diffraction spikes (Figure 1). Each galaxy had two images for two different filters: F606W and F814W.

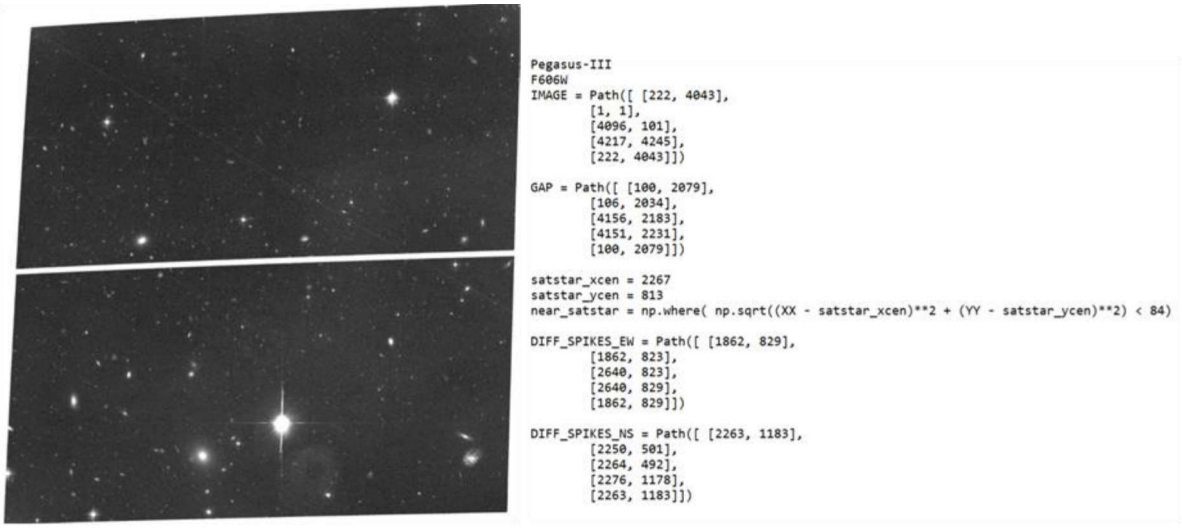

```
Pegasus-III
F606W
IMAGE = Path([ [222, 4043],
       [1, 1],
       [4096, 101],
       [4217, 4245],
       [222, 4043]])

GAP = Path([ [100, 2079],
       [106, 2034],
       [4156, 2183],
       [4151, 2231],
       [100, 2079]])

satstar_xcen = 2267
satstar_ycen = 813
near_satstar = np.where( np.sqrt((XX - satstar_xcen)**2 + (YY - satstar_ycen)**2) < 84)

DIFF_SPIKES_EW = Path([ [1862, 829],
       [1862, 823],
       [2640, 823],
       [2640, 829],
       [1862, 829]])

DIFF_SPIKES_NS = Path([ [2263, 1183],
       [2250, 501],
       [2264, 492],
       [2276, 1178],
       [2263, 1183]])
```

Figure 1. Sample F606W image of dwarf galaxy Pegasus III (left) and sample document of coordinates used for masking (right).

2.2. *Hercules*

Using a data table for the Hercules galaxy and the paper *The Star Formation History and Extended Structure of the Hercules Milky Way Satellite* (Sand et al. 2009), we created plots for right ascension (RA) / declination with and without data cuts, color-magnitude diagrams (CMDs), and 15 Gyr isochrones. We compared these plots with those shown in the paper to confirm their accuracy. Visualizing this data is important for characterizing old, metal-poor galaxies as their ages and metallicities can tell us about their evolutions.

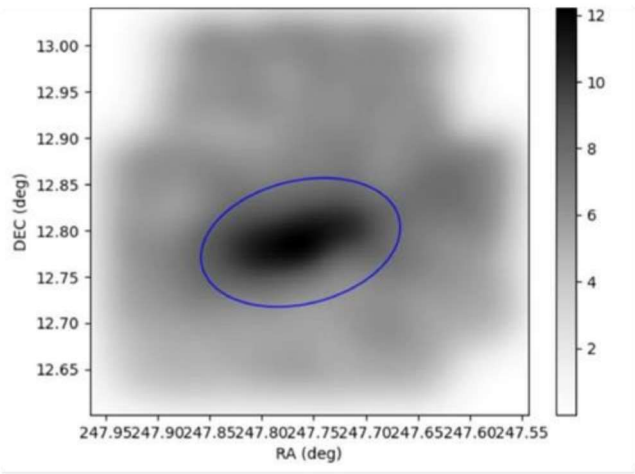

Figure 2. Density plot of RA and declination. Ellipse shows the main concentration of mass using a half-light radius of 5.9 arcminutes (Sand et al. 2009).

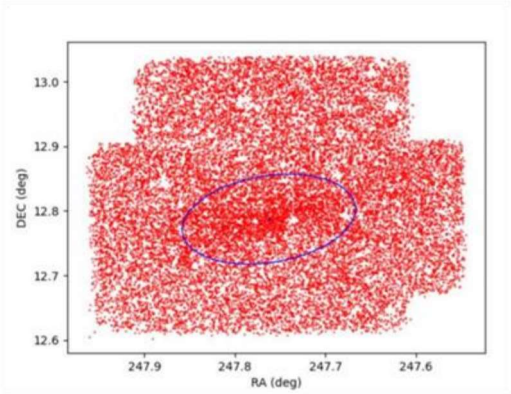

Figure 3. Scatter plot of right ascension (RA) and declination. Ellipse shows the main concentration of mass using a half-light radius of 5.9 arcminutes (Sand et al. 2009).

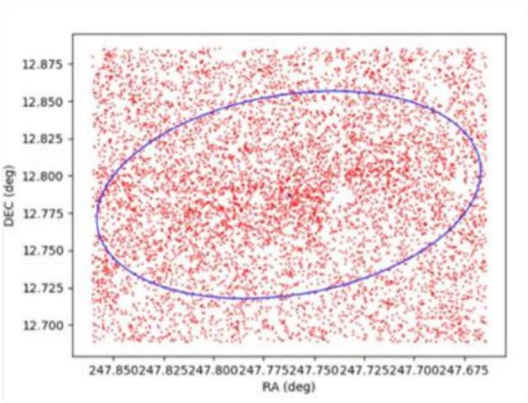

Figure 4. Plot of RA and declination with radial distance and magnitude data cuts. Ellipse shows the main concentration of mass using a half-light radius of 5.9 arcminutes (Sand et al. 2009).

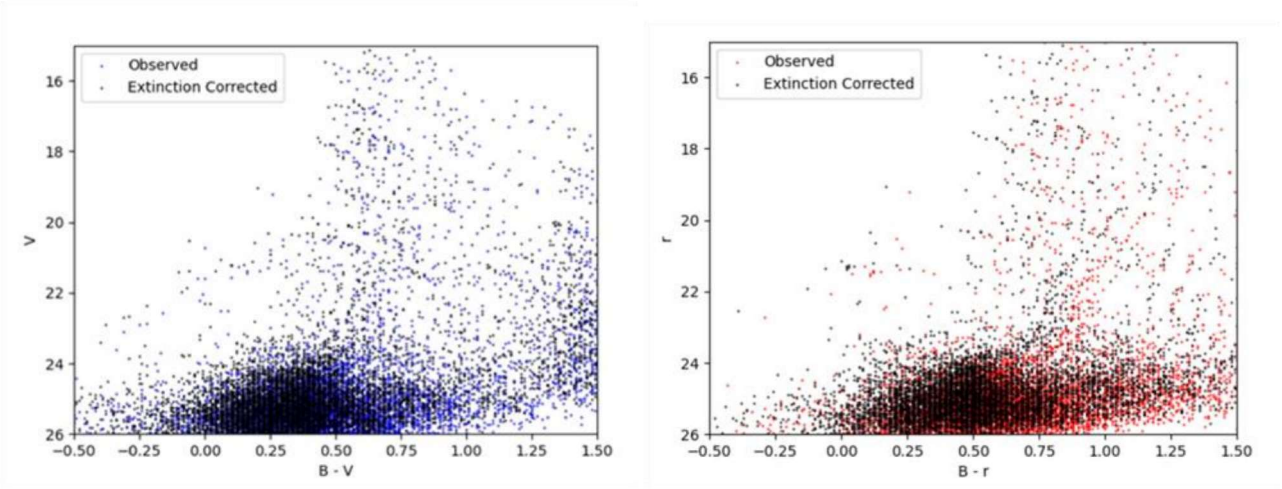

Figure 5. CMD plots with radial distance and magnitude data cuts. Both observed and extinction-corrected values shown. Left: B-V CMD. Right: B-r CMD.

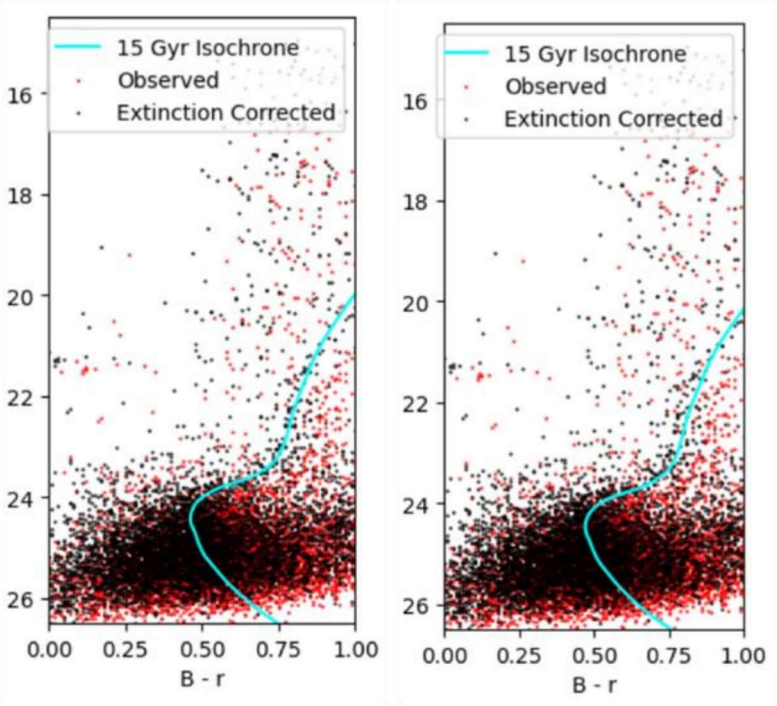

Figure 6. Plots of 15 Gyr isochrones overlayed on B-r plot. Left: $[Fe/H] = -2.49$ isochrone from Dotter et al. (2008). Right: $[Fe/H] = -2.3$ isochrone from Girardi et al. (2004).

2.3. *Eridanus II*

Using the paper *Eridanus II: A Fossil From Reionization With An Off-Center Star Cluster* (Simon et al. 2020) and a Python program for Markov Chain Monte Carlo (MCMC) fitting, we tested the impact of altering different structural parameters of the Eridanus II galaxy on the resulting half-light radius (extension). Specifically, we altered the values of initial model parameters *position angle* and *ellipticity* as well as the number of *bins* used to cover the Eridanus II image. We then tested all of these changes using a Plummer profile for normalization and using an Exponential profile.

2.4. *Pegasus III*

Similarly to Eridanus II, we used an MCMC Python program to test the effect of different magnitude depths on the resulting values and error ranges of *position angle*,*ellipticity*, and *half-light radius*. These were tested with both Plummer and Exponential profiles as well.

Table 1. Eridanus II - Position Angle versus Extension (Half-Light Radius)

Profile	Position Angle (degrees)	Extension (arcminutes)	Extension Error Upper (arcminutes)	Extension Error Lower (arcminutes)
(6)	(7)	(8)	(9)	(10)
	30	3.345033627	0.081615826	0.077474154
	35	3.338834924	0.082522715	0.076371126
	40	3.75665741	0.120779488	0.109325105
*Plummer	45	4.01551152	0.142112408	0.133358813
	60	4.330585678	0.178457359	0.164081303
	**72.6	4.339641785	0.172423121	0.160639143
	80	4.335428478	0.177732096	0.158333967
	100	4.280497799	0.167910008	0.154362196
	30	3.554335566	0.116961896	0.111773976
	35	3.769775305	0.138798901	0.128219365
	40	4.045267179	0.158949658	0.152502337
Exponential	45	4.362393579	0.197776305	0.18403778
	60	4.823635012	0.259568593	0.225663266
	**72.6	4.832967168	0.256250936	0.22102263
	80	4.824943169	0.259031281	0.23347696
	100	4.812160763	0.250344985	0.224389511

NOTE— *This is the default profile used.
**This is the default position angle value used.

Table 2. Eridanus II - Ellipticity versus Extension (Half-Light Radius)

Profile	Ellipticity	Extension (arcminutes)	Extension Error Upper (arcminutes)	Extension Error Lower (arcminutes)
(6)	(7)	(8)	(9)	(10)
	0.11	4.328100094	0.175159187	0.160095299
	0.2	4.325642118	0.172423121	0.160639143
*Plummer	**0.41	4.339641785	0.17523861	0.158535143
	0.6	4.323670099	0.176314077	0.165293718
	0.89	4.33901132	0.173872446	0.158931879
	0.11	4.828316859	0.266241811	0.231568027
	0.2	4.832316693	0.256250936	0.22102263
Exponential	**0.41	4.832967168	0.263457531	0.22827376
	0.6	4.821458738	0.263457531	0.22827376
	0.89	4.821458738	0.257355697	0.225947089

NOTE— *This is the default profile used.
**This is the default ellipticity value used.

Table 3. Eridanus II - Bins versus Extension (Half-Light Radius)

Profile	Bins	Extension (arcminutes)	Extension Error Upper (arcminutes)	Extension Error Lower (arcminutes)
(1)	(2)	(3)	(4)	(5)
*Plummer	100	4.309265189	0.1759676	0.154958141
	150	4.290984829	0.172385395	0.152373233
	200	4.315393833	0.170607886	0.16342472
	250	4.331966041	0.176201063	0.157724065
	**268	4.339641785	0.172423121	0.160639143
	300	4.321140158	0.17174498	0.157227306
Exponential	100	4.767910659	0.249622869	0.219984942
	150	4.759997743	0.249757658	0.226571647
	200	4.79820681	0.256213014	0.225262509
	250	4.81911134	0.249901022	0.235005938
	**268	4.832967168	0.256250936	0.22102263
	300	4.818366293	0.257067822	0.225683351

NOTE— *This is the default profile used.
**This is the default bins value used.

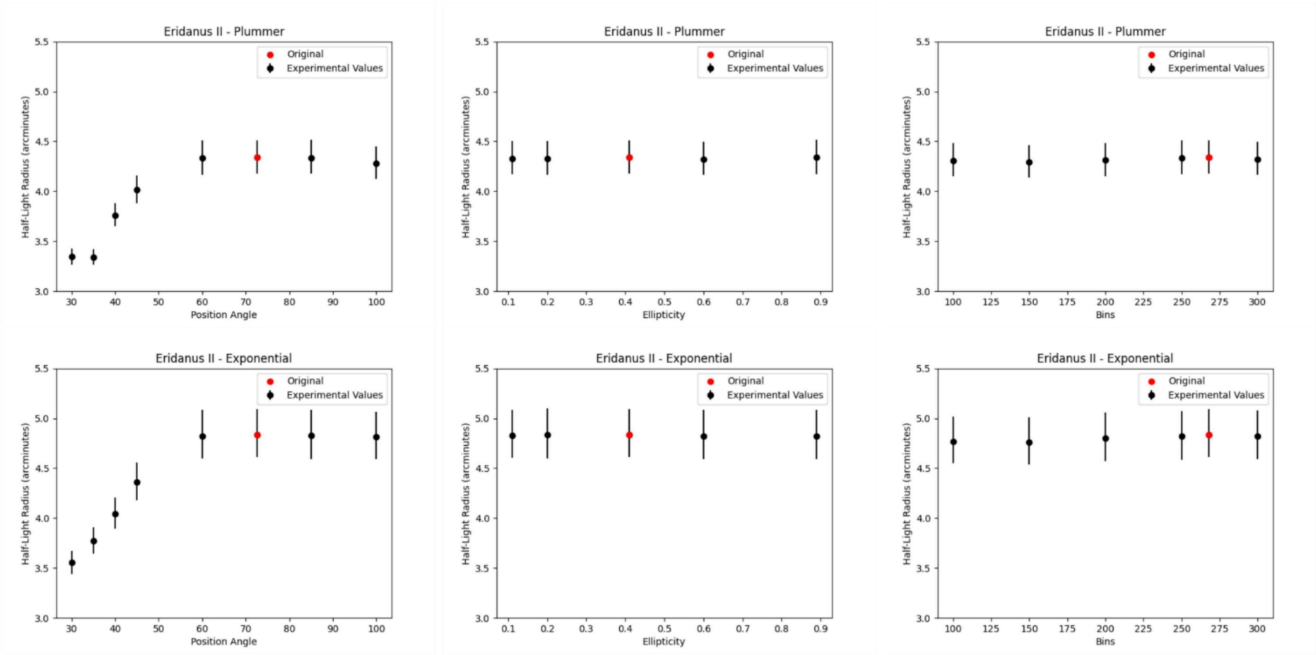

Figure 7. Eridanus II - Resulting half-light radius (extension) values and their errors for varying values of position angle (left), ellipticity (middle), and bins (right). Top: Plummer profile. Bottom: Exponential profile.

Table 4. Pegasus III - Effect of Magnitude Depth on Error Values

Profile	Magnitude	Position Angle (degrees)	Position Angle Error Upper	Position Angle Error Lower	Ellipticity	Ellipticity Error Upper	Ellipticity Error Lower	Extension (arcminutes)	Extension Error Upper (arcminutes)	Extension Error Lower(arcminutes)
(1)	(2)	(3)	(4)	(5)	(6)	(7)	(8)	(9)	(10)	(11)
	26.5	190.6694054	6.57754996	11.22402626	0.368677596	0.177940888	0.15718003	2.365033094	1.09401137	0.60667132
*Plummer	**27	188.5658093	7.297522357	9.536685917	0.127103494	0.379495991	0.128476372	2.093169367	0.694686412	0.468332875
	27.5	186.20007	9.313915436	12.32027328	0.106206541	0.273376497	0.102777996	1.615826084	0.38041491	0.294267614
	***30	184.3989697	9.396894654	9.830217802	0.100140281	0.29948316	0.097866884	1.582597452	0.323307316	0.256234171
	26.5	190.4692617	6.806790029	10.70235715	0.361184369	0.167950575	0.154529988	2.583070929	1.146910728	0.724851963
Exponential	**27	188.610383	7.463402861	9.945486157	0.359173636	0.123916378	0.119047725	2.265507926	0.73840494	0.562510836
	27.5	187.1119224	8.395978222	11.59565839	0.283870717	0.112711939	0.108018513	1.812898743	0.558908116	0.43130885
	***30	185.8904807	8.491199471	10.30792663	0.299528541	0.103666206	0.101724498	1.769907494	0.515073005	0.376661632

NOTE— *This is the default profile used.
**This is the default magnitude value used.
***Represents no cuts.

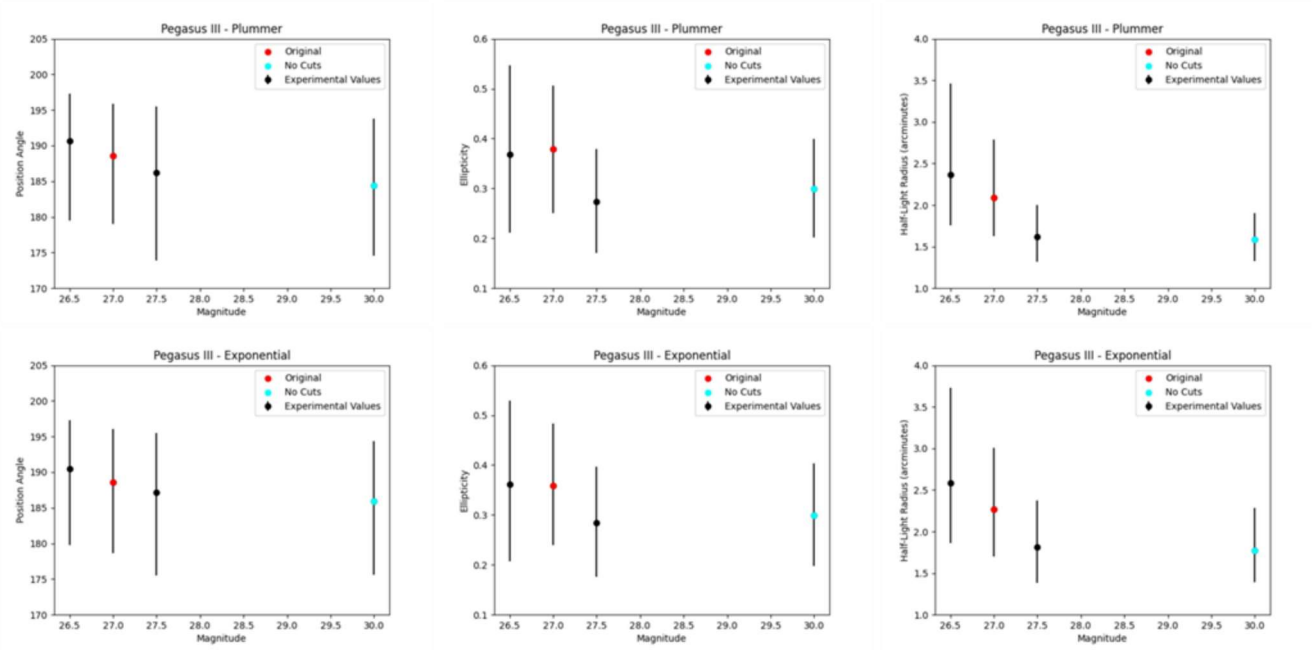

Figure 8. Pegasus III - Resulting values and their errors of position angle (left), ellipticity (middle), and bins (right) against varying values for magnitude. Top: Plummer profile. Bottom: Exponential profile.

Table 5. Eridanus II - Means and Standard Deviations of Extension for Modified Parameters

Profile	Parameter Modified	Extension Mean	Extension Standard Deviation
(1)	(2)	(3)	(4)
Plummer	Position Angle	3.967773902625	0.40821302216815
	Ellipticity	4.3312130832	0.0067746361803802
	Bins	4.3180653058333	0.015738279534045
Exponential	Position Angle	4.378184717625	0.49410958417001
	Ellipticity	4.8273036392	0.0050310758552971
	Bins	4.7994266688333	0.027143286004161

Table 6. Pegasus III - Means and Standard Deviations of Parameters from Modifying Magnitude

Profile	Position Angle Mean	Position Angle Standard Deviation	Ellipticity Mean	Ellipticity Standard Deviation	Extension Mean	Extension Standard Deviation
(8)	(9)	(10)	(11)	(12)	(13)	(14)
Plummer	187.4585636	2.3706760153463	0.330258311	0.044952867746944	1.91415649925	0.32949497302311
Exponential	188.02051195	1.7107667352754	0.32593931575	0.034691605053524	2.107846273	0.33611468812822

3. ANALYSIS

The masking of HST images will be used for future examination of these galaxies and does not require further analysis. The Hercules plots are a recreation of data from Sand et al. (2009) and reinforce their validity.

For the Eridanus II MCMC program, modifying certain parameters impacted the resulting extension more dramatically than others. As shown in Table 5, modifications to the position angle resulted in much larger standard deviations than modifying the other two parameters, ellipticity and bin number. Table 1 shows that position angles below 45 showed a large drop in extension, the lower angles resulting in half-light radii an entire arcminute smaller than the original for the Plummer profile and well over a full arcminute in the Exponential case. Changing ellipticity and bin number provided much more consistent results.

With the Eridanus II data, all cases of parameter modification showed larger half-light radii when run with the Exponential profile than with the Plummer profile. For position angle, ellipticity, and bins, the mean values returned for the Exponential case were roughly half an arcminute larger than those returned for Plummer. The change in profiles did not seem to affect the standard deviations significantly.

Pegasus III data shows that modifying magnitude values for the MCMC program tended to return smaller position angles, ellipticities, and extensions as the magnitude got larger (Table 4). Figure 8 and Table 6 show that the use of Plummer versus Exponential profiles did not have a significant effect on the results of position angle or ellipticity. Similarly to the Eridanus II data, however, the Exponential profile gave larger values for extension (approximately 0.2 arcminutes larger in each case).

4. CONCLUSION

The image masking will provide valuable tools for future studies. Coordinates like those obtained during the masking process were used in the MCMC programs for Eridanus II and Pegasus III, so documents such as the one shown in Figure 1 may be used to model other galaxies in a similar way. Recreating the Hercules plots confirms their validity and shows how radial and magnitude data cuts narrows down samples more effectively. The data from Eridanus II shows that modifying the initial position angle value has a significant effect on the resulting half-light radius, especially for lower PA values. Modifying ellipticity and bin numbers has less of an impact, however using an Exponential profile as opposed to the default Plummer profile returns larger values overall. Interestingly, using an Exponential profile for Pegasus III had the same effect of augmenting extension results that it did for Eridanus II. Position angle and ellipticity results stayed consistent between the two profiles, and a major trend in the data was the decrease in all values as the provided magnitude depth got larger. The most significant takeaways from this data is the significant effect of initial position angle on half-light radius, the amplification of half-light radius values when using an Exponential profile rather than a Plummer profile, and the negative correlation between magnitude depth and position angle, ellipticity, and half-light radius.

REFERENCES

Bechtol, K., Drlica-Wagner, A., Balbinot, E., et al. 2015, ApJ, 807, 50, doi: 10.1088/0004-637X/807/1/50

Drlica-Wagner, A., Bechtol, K., Rykoff, E. S., et al. 2015, ApJ, 813, 109, doi: 10.1088/0004-637X/813/2/109

Drlica-Wagner, A., Bechtol, K., Allam, S., et al. 2016, ApJL, 833, L5, doi: 10.3847/2041-8205/833/1/L5

Homma, D., Chiba, M., Okamoto, S., et al. 2018, PASJ, 70, S18, doi: 10.1093/pasj/psx050

Kallivayalil, N., Sales, L. , Zivick, P. et al. 2018, ArXiv e-prints. https://arxiv.org/abs/1805.01448

Kim, D., Jerjen, H. 2015, ApJL, 808, L39, doi: 10.1088/2041-8205/808/2/L39

Kim, D., Jerjen, H., Mackey, D., Da Costa, G. S., Milone, A. P. 2015, ApJL, 804, L44, doi: 10.1088/2041-8205/804/2/L44

Koposov, S. E., Belokurov, V., Torrealba, G., Evans, N. W. 2015a, ApJ, 805, 130, doi: 10.1088/0004-637X/805/2/130

Koposov, S. E., Walker, M. G., Belokurov, V., et al. 2018, ArXiv e-prints. https://arxiv.org/abs/1804.06430

Laevens, B. P. M., Martin, N. F., Bernard, E. J., et al. 2015a, ApJ, 813, 44, doi: 10.1088/0004-637X/813/1/44

Martin, N. F., Nidever, D. L., Besla, G., Olsen, K., et al. 2015, ApJL, 804, L5, doi: 10.1088/2041-8205/804/1/L5

Sand, D., Olszewski, E. , Willman, B. et al. 2009, ArXiv e-prints. https://arxiv.org/abs/0906.4017

Simon, J., Brown, T. , Drlica-Wagner, A. et al. 2020, ArXiv e-prints. https://arxiv.org/abs/2012.00043

Torrealba, G., Koposov, S. E., Belokurov, V., Irwin, M. 2016a, ArXiv e-prints. https://arxiv.org/abs/1601.07178

Torrealba, G., Koposov, S. E., Belokurov, V., et al. 2016b, MNRAS, 463, 712, doi: 10.1093/mnras/stw2051

Torrealba, G., Belokurov, V., Koposov, S. E., et al. 2018, MNRAS, 475, 5085, doi: 10.1093/mnras/sty170